

Wiring cost and topological participation of the mouse brain connectome

Mikail Rubinov^{a,b,1,2}, Rolf J. F. Ypma^{a,c,1}, Charles Watson^{d,e}, and Edward T. Bullmore^{a,f,g}

^aBehavioural and Clinical Neuroscience Institute, Department of Psychiatry, University of Cambridge, Cambridge CB2 3EB, United Kingdom; ^bChurchill College, University of Cambridge, Cambridge CB3 0DS, United Kingdom; ^cHughes Hall, University of Cambridge, Cambridge CB1 2EW, United Kingdom;

^dNeuroscience Research Australia, University of New South Wales, Sydney NSW 2031, Australia; ^eFaculty of Health Sciences, Curtin University, Kent Street, Bentley, WA 6102, Australia; ^fCambridgeshire and Peterborough NHS Foundation Trust, Huntingdon PE29 3RJ, United Kingdom; and ^gAlternative Discovery and Development, GlaxoSmithKline, Stevenage SG1 2NY, United Kingdom

Edited by Marcus E. Raichle, Washington University in St. Louis, St. Louis, MO, and approved July 6, 2015 (received for review October 22, 2014)

Brain connectomes are topologically complex systems, anatomically embedded in 3D space. Anatomical conservation of “wiring cost” explains many but not all aspects of these networks. Here, we examined the relationship between topology and wiring cost in the mouse connectome by using data from 461 systematically acquired anterograde-tracer injections into the right cortical and subcortical regions of the mouse brain. We estimated brain-wide weights, distances, and wiring costs of axonal projections and performed a multiscale topological and spatial analysis of the resulting weighted and directed mouse brain connectome. Our analysis showed that the mouse connectome has small-world properties, a hierarchical modular structure, and greater-than-minimal wiring costs. High-participation hubs of this connectome mediated communication between functionally specialized and anatomically localized modules, had especially high wiring costs, and closely corresponded to regions of the default mode network. Analyses of independently acquired histological and gene-expression data showed that nodal participation colocalized with low neuronal density and high expression of genes enriched for cognition, learning and memory, and behavior. The mouse connectome contains high-participation hubs, which are not explained by wiring-cost minimization but instead reflect competitive selection pressures for integrated network topology as a basis for higher cognitive and behavioral functions.

conservation law | viral tracing | graph theory | cytoarchitectonics | transcriptomics

Network organization of the brain is fundamental to the emergence of complex neuronal dynamics, cognition, learning, and behavior. Modern concepts of anatomical network connectivity originated in the 19th and early 20th century with the ascendancy of the neuron theory: the concept of discrete nerve cells contiguously connected via axonal projections and synaptic junctions (1, 2). In the last decade, the connectome has emerged as a new word to define the complete structural “wiring diagram” of a nervous system or brain (3). At the small scale of synaptically connected neurons, the connectome has only been completely mapped for the 302-neuron nervous system of the roundworm *Caenorhabditis elegans*, using serial electron microscopy and painstaking visual synaptic reconstruction (4). At the large scale of axonally connected brain regions, draft connectomes have been mapped for the cat and macaque, by collation of primary tract-tracing studies (5–7), and for the human, using *in vivo* diffusion-weighted magnetic resonance imaging measures of white matter tract organization (8), or interregional covariation measures of cortical thickness or volume (9).

Topological analyses of these connectomes have consistently demonstrated a repertoire of complex network properties, including the simultaneous presence of modules and hubs (10). The seemingly ubiquitous appearance of these topological features, e.g., both at the cellular scale of the worm brain and at the areal scale of the human brain, supports scale- and species-invariant organizational principles of nervous systems, consistent with Ramón y Cajal’s seminal “laws of conservation for time,

space and material” (1, 11–13). Anatomically localized and functionally specialized modules conserve space and (biological) material by reducing the average length of axonal projections, or wiring cost; anatomically distributed and functionally integrative hubs conserve (conduction) time by reducing the average axonal delay, or speed of interneuronal communication. The simultaneous presence of modules and hubs supports a contemporary reformulation of Ramón y Cajal’s laws as a trade-off between minimization of wiring cost and maximization of topological integration.

Magnetic resonance imaging (MRI) allowed for testing such organizational principles in large-scale mammalian connectomes with high throughput whole-brain imaging. However, MRI methods measure anatomical connectivity indirectly and at low (millimeter scale) spatial resolution (14). In contrast, tract tracing methods measure anatomical connectivity directly, by detecting axonally mediated propagation of injected tracer, and at higher (micrometer scale) spatial resolution. Tract-tracing methods represent the current “gold standard” for mapping mammalian connectomes. However, most tract-tracing connectome studies to date have been limited to metaanalyses of primary datasets with limited brain

Significance

We analyzed a large dataset of tract tracing experiments to investigate the topological and spatial properties of the mouse brain connectome. We found expensive, topologically integrative hub nodes, which could not be explained by global minimization of wiring cost alone. These “high-participation” hubs mediated communication between functionally specialized and anatomically localized network modules and were associated with high expression of genes involved in cognitive and behavioral processes. We propose that the mouse brain network is selected by simultaneous competitive pressures for wiring-cost minimization and hub-mediated information exchange between network modules. High-participation hubs are expensive but central to global integration of information and, thus, essential for adaptive “higher order” brain functions.

Author contributions: M.R., R.J.F.Y., and E.T.B. designed research; M.R. and R.J.F.Y. performed research; M.R. and R.J.F.Y. contributed new reagents/analytic tools; M.R., R.J.F.Y., C.W., and E.T.B. analyzed data; M.R., R.J.F.Y., C.W., and E.T.B. wrote the paper; M.R. processed the connectivity and gene-expression data, defined nodes, distances, and costs, constructed topological and physical connectomes, and performed community, core, participation, and modeling analyses; R.J.F.Y. mapped the cytoarchitectonic data, performed gene-expression, cytoarchitectonic, robustness, and validation analyses, and created visualizations; M.R. and R.J.F.Y. defined edges and fitted weight-distance relationships; C.W. provided advice on the developmental ontology and interpretation of modules; and E.T.B. conceived and supervised the project.

Conflict of interest statement: E.T.B. is employed 50% by the University of Cambridge and 50% by GlaxoSmithKline (GSK); he holds stock in GSK.

This article is a PNAS Direct Submission.

¹M.R. and R.J.F.Y. contributed equally to this work.

²To whom correspondence should be addressed. Email: mr572@cam.ac.uk.

This article contains supporting information online at www.pnas.org/lookup/suppl/doi:10.1073/pnas.1420315112/-DCSupplemental.

coverage and variable definitions of brain regions and interregional connections (6, 7). Tract-tracing methods for comprehensive and systematic mapping of the connectome did not exist until recently (15–18).

The recent step change in the quality and quantity of available tract-tracing measurements in mammalian species, such as the macaque and the mouse, provides a crucial opportunity to test theories of connectome organization more rigorously. Some of the first systematic high-quality tract tracing studies in the macaque have revealed many previously unreported weak and long-range axonal projections (19, 20). These studies have also shown that spatial constraints on wiring cost, modeled by an exponential decay weight–distance relationship, can account for many important aspects of the macaque connectome (21, 22).

We therefore considered it important to comprehensively evaluate the design principles of the mouse connectome in a systematically acquired dataset of axonal tract-tracing experiments (17). We measured the topological and spatial properties of this connectome and compared these properties to equivalent properties of reference lattice and random graphs. We hypothesized that the connectome would have a complex topology and include integrative hubs inexplicable by minimization of wiring cost. We also explored the neurobiological substrates of the mouse connectome by correlating topological properties with histological and gene-expression properties quantified from independently acquired datasets.

Results

We studied the topological and spatial properties of the mouse connectome, using data on 461 axonal tract-tracing experiments in wild-type mice, conducted and made publicly available by the Allen Institute for Brain Science (17, 23, 24). We used topographical and developmental mouse-brain ontologies (25) to subdivide the whole mouse brain into 130 bilaterally symmetric cortical and subcortical regions. Each experiment consisted of an anterograde tracer injection into one of the 65 regions on the right side of the brain, followed by whole-brain (intrahemispheric and interhemispheric) mapping of axonal projections. We defined weights of directed interregional axonal projections (edges) as normalized connection densities (NCD), discarded nine nodes on each side of the brain that had no available experiments, and removed spurious connections by using a probabilistic threshold ($P < 0.01$) based on expert visual review of tract-tracing images (17). We assumed hemispheric symmetry and used the available interhemispheric projections to construct a whole-brain connectome (Fig. 1A and B, *SI Appendix*, and Dataset S1).

The resulting anatomical connectivity matrix had 112 nodes, a connection density of 53% (i.e., approximately half of all possible interareal connections existed), and an approximately symmetrical, block-diagonal appearance (Fig. 1D). The interregional NCD weights were highly heterogeneous and followed a log-normal distribution: the strongest edges had NCD four orders of magnitude greater than the weakest edges. The sum of edge weights connecting a given node to the rest of the network (nodal strength) also followed a log-normal distribution. We defined two measures of cost: the axonal distance (in millimeters) of interregional projections, estimated by continuous axonal tract reconstruction from images of tracer propagation, and the axonal wiring cost of interregional projections, computed as the product of axonal distance and the normalized axonal bandwidth. The bandwidth is a marker of axonal cross-sectional area, and axonal wiring cost therefore approximates the normalized volume of a cylindrical axonal projection (Fig. 1B–F and *SI Appendix*).

NCD weights of axonal projections w decayed as a function of interregional distance d (17). The form of this weight–distance relationship was significantly better fit by a power law, $w \propto d^{-\alpha}$, than by an exponential function $w \propto e^{-\beta d}$ ($P < 10^{-6}$, Vuong's

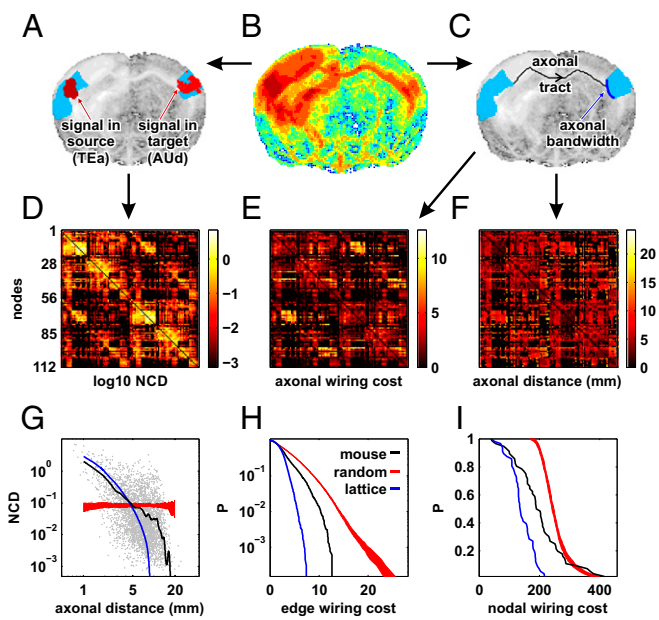


Fig. 1. Connectivity and costs of the mouse connectome. (A–C) Illustration of projection of tracer signal in one experiment (Allen Institute ID 157062358), coronal view. (A) Tracer injected into a source region (temporal association areas, TEa) was axonally transported to a target region (dorsal auditory area, AUDd). Connection weight was estimated with the normalized connection density (NCD), defined as the signal density in the target region (AUDd, red voxels) divided by the density of tracer injected in the source region (TEa, red voxels). (B) Image of tracer signal intensity on logarithmic scale. (C) Axonal distance was defined as the shortest estimated distance of the directed axonal projection from source to target (solid black line); normalized axonal bandwidth was defined as the proportion of the target's boundary that shows signal (solid navy line); wiring cost was defined as the product of axonal distance and bandwidth. (D–F) Matrices of interregional NCD, wiring cost, and axonal distance ordered by block diagonalization of the NCD matrix. (G) Scatter plot of the NCD weight–distance relationship in the connectome, and locally smoothed weight–distance relationships in the connectome, lattice, and random graphs (solid lines). (H and I) Cumulative probability distributions of wiring cost of edges and nodes in the connectome, lattice, and random graphs. Confidence intervals for random graphs are interquartile ranges estimated from 100 random networks.

test). The power law for global weight–distance scaling in the connectome had an exponent of 2.05, such that $w \propto d^{-2.05}$, and clearly differed both from the exponential weight–distance scaling of a 3D spatial lattice (constructed by assigning strongest weights to closest pairs of nodes and, thereby, globally minimizing axonal wiring cost), and from the absent weight–distance scaling of random graphs (constructed by assigning weights to random pairs of nodes) (Fig. 1G). The connectome had a higher probability of high-cost nodes and edges compared with the spatial lattice but a lower probability of high-cost nodes and edges compared with the random graph (Fig. 1H and I).

We characterized the global organization of the connectome by computing the topological measures of average shortest path length and clustering coefficient, and their normalized ratio known as the small-world index, σ . Simultaneously low path length and high clustering give $\sigma > 1$, and define small worldness, a marker of complex network topology. We found $\sigma > 1$ across a range of network densities, up to and including the studied 53%, establishing that the dense, weighted, and directed mouse connectome is a small-world network; see *SI Appendix* for additional discussion.

We detected a stable community structure of the connectome, using a multiscale modular decomposition (Fig. 2, *SI Appendix*, Table S1, and Movie S1). We found that 48 of the 56 bilaterally symmetric nodes could be reliably classified into four modules.

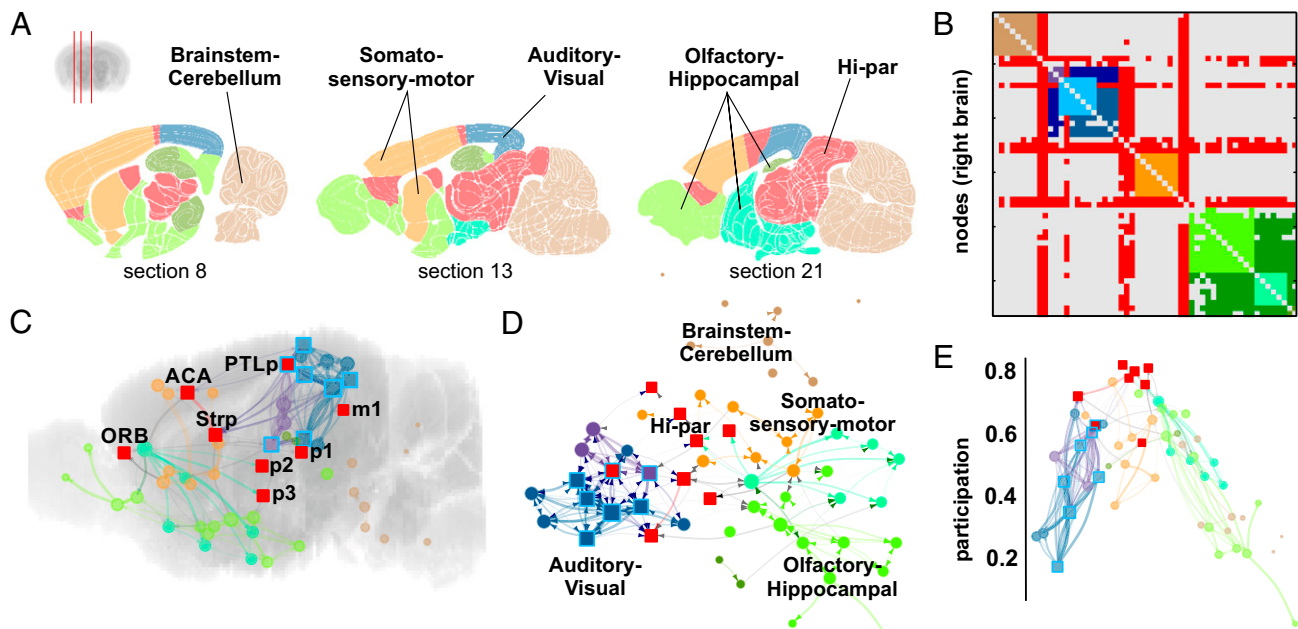


Fig. 2. Community structure of the mouse connectome. Representations of hierarchical modules, core and high-participation, or hi-par, hubs. (*A*) Anatomical representation in sagittal sections with regions color-coded according to modular affiliation. Hi-par regions are in red. Sections are numbered as in the Allen Reference Atlas, mouse.brain-map.org/static/atlas; *Inset* shows section locations in coronal plane. (*B*) Connectivity matrix representation with blocks of hierarchical modules, the core embedded in the auditory-visual module (cyan), and intermodular connections mediated by hi-par hubs (red). (*C–E*) Graph representations with nodes arranged either in anatomical space (*C*), in topological space (force-directed graph layout) (*D*), or with nodes vertically arranged according to values of participation (*E*). Nodes are color-coded by modular affiliation; core nodes are squares with cyan borders; hi-par hubs are red squares. ACA, anterior cingulate area; Al, agranular insular area; GU, gustatory areas; m1, midbrain (mesomere 1); MOp, primary motor area; MOs, secondary motor area; ORB, orbital area; p1, prectectum (prosomere 1); p2, thalamus (prosomere 2); p3, prethalamus (prosomere 3); PTLp, posterior parietal association areas; SSs, primary somatosensory area; SSs, supplemental somatosensory area; Stri, intermediate stratum of striatum; Strp, caudate nucleus (periventricular stratum of striatum); VISC, visceral area.

Two of the four modules were further divisible into submodules, reflecting a hierarchically modular organization of functionally specialized brain regions. At the highest level of the hierarchy the four modules comprised: (*i*) a somatosensory-motor module; (*ii*) a brainstem-cerebellum module; (*iii*) an auditory-visual module subtending auditory and visual submodules; and (*iv*) an olfactory-hippocampal-hypothalamic module subtending olfactory, hippocampal, and hypothalamic submodules. The connectome could also be decomposed into a stable core of high-strength nodes and a periphery of low-strength nodes. The core comprised seven highest-strength nodes (ventral auditory area; anterolateral, anteromedial, lateral, and posterolateral visual areas; temporal and posterior parietal association cortex), all located in the auditory-visual module.

Participation coefficient p , a measure of connection diversity ($0 < p < 1$), was generally low for nodes reliably assigned to hierarchical modules, $p = 0.50 \pm 0.17$ (SD), indicating that these nodes tended to have more intramodular than intermodular connections. In contrast, eight nodes in the network (orbital, anterior cingulate, posterior parietal association cortex, caudate nucleus, prethalamus, thalamus, prectectum, and midbrain) were not reliably assigned to hierarchical modules and had diverse connections indicated by significantly higher ($P < 0.001$, Wilcoxon rank-sum test) participation coefficients, $p = 0.77 \pm 0.07$ (SD). We termed these eight nodes “high-participation” (hi-par) hubs. One hi-par hub, posterior parietal association cortex, was also in the core.

Participation positively correlated with nodal degree and wiring cost (Fig. 3 *A* and *B*). Participation also correlated with weight-distance power-law exponents, estimated individually for each node, and there was a significant difference ($P = 0.011$, Wilcoxon rank-sum test) in the average power-law exponent for hi-par nodes, $\hat{\alpha}_{\text{hi-par}} = 1.75 \pm 0.72$ (SD), compared with the average exponent

for low-participation (lo-par) nodes, $\hat{\alpha}_{\text{lo-par}} = 2.47 \pm 0.63$ (SD). In other words, connection weights of hi-par nodes decayed slower as a function of distance (Fig. 3 *C–E*). We used the global weight-distance scaling relationship $w_{\text{global}} \propto d^{-2.05}$ (Fig. 3*D*) to algorithmically bipartition the connectome into low-cost and high-cost subnetworks, such that the low-cost subnetwork predominantly contained weights $w_{\text{low-cost}} < w_{\text{global}}$, and the high-cost subnetwork predominantly contained weights $w_{\text{hi-cost}} > w_{\text{global}}$ (26). The low-cost subnetwork comprised mainly lo-par nodes, and the high cost subnetwork comprised most of the core and hi-par nodes (Fig. 3*F* and *SI Appendix*, Table S1).

We used three deterministic network models to simulate the topological organization of the connectome (Fig. 3 *G–I*). First, the nonparametric cost-minimized spatial lattice generated a moderately similar community structure to the connectome (normalized mutual information, $NMI = 0.66$) including modules and a core, but no hi-par hubs (Fig. 3*H*). Second, a one-parameter model counterpart of global cost minimization, $w \propto d^{-2.05}$, generated a network broadly similar to the lattice. Third, a topologically adaptive model that assigned weights to edges based on each node’s individual weight-distance power-law exponent (and, thus, assigned strong, long, and costly edges to hi-par nodes) generated hierarchical modules, a core, and seven hi-par hubs (Fig. 3*I*). The topologically adaptive model also showed a more similar community structure ($NMI = 0.69$) and substantially higher correlations (compared with the lattice) with many other connectome statistics, including connection weight ($r = 0.51$ in the lattice model, compare $r = 0.64$ in the topologically adaptive model), nodal degree ($r = 0.47$ compare $r = 0.82$), nodal strength ($r = 0.73$ compare $r = 0.90$) and nodal participation ($r = 0.42$ compare $r = 0.64$).

We finally explored neurobiological substrates of hi-par nodes by using histological and gene-expression measures quantified from

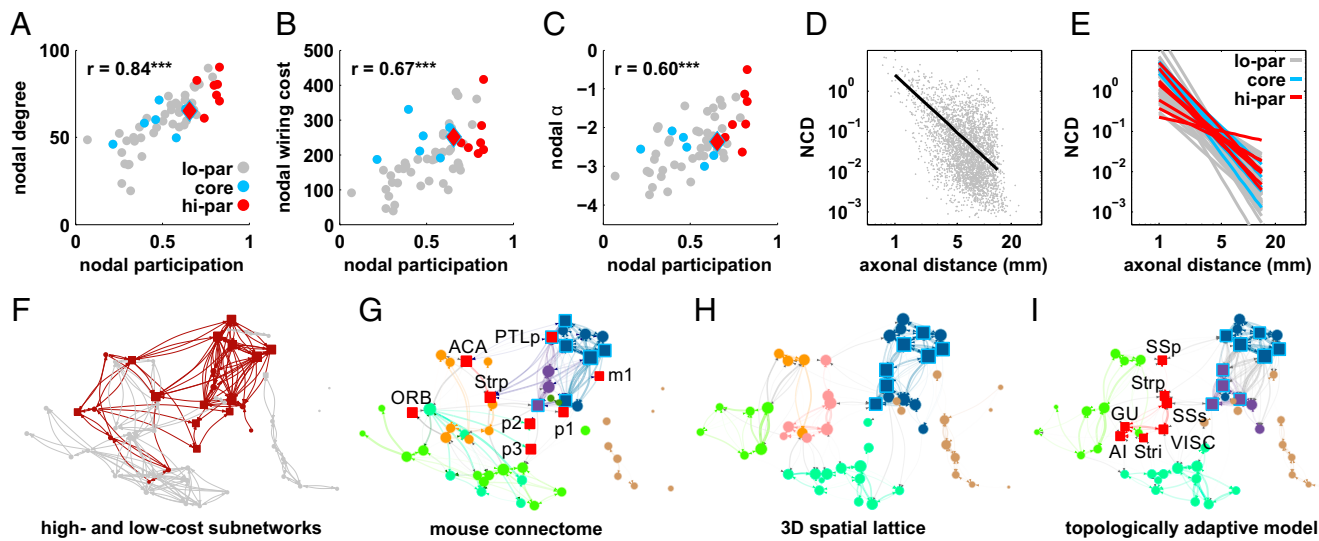


Fig. 3. High-participation hubs are expensive. (A–C) Scatterplots of participation coefficient versus degree, wiring cost, power-law exponent α for lo-par (gray), core (cyan), and hi-par (red) nodes (diamonds show posterior parietal association cortex, which is simultaneously a core and a hi-par node). *** $P < 0.001$ (D and E) Weight–distance scaling fits for the whole network (D), and for lo-par, core and hi-par nodes (E), estimated from weight–distance scatter plots of individual nodes. Graph representations in anatomical space of the high-cost subnetwork (brown) and low-cost subnetwork (gray) (F), the connectome (G), in the cost-minimized lattice (H), and the topologically adaptive model (I). See Fig. 2 for regional abbreviations.

independently acquired datasets. We correlated nodal participation with nodal neuronal density, neuronal and nonneuronal cell counts, and cortical thickness, using previously published data for neocortical regions (27) (*SI Appendix*, Table S12). Participation negatively correlated with neuronal volume density ($r = -0.66, P < 0.001$), neuronal surface density ($r = -0.60, P = 0.002$), and fraction of neurons in the total cell population ($r = -0.59, P = 0.003$); in contrast, strength positively correlated with neuronal volume density ($r = 0.64, P = 0.001$) (Fig. 4A and *SI Appendix*, Fig. S9). These results, as well as the related negative correlation between degree and neuronal volume density ($r = -0.48, P = 0.02$), are compatible with the negative (albeit nonsignificant) correlation between strength and participation of neocortical regions ($r = -0.32, P = 0.14$), and with simultaneously high neuronal density and low participation of high-strength core regions (*SI Appendix*, Figs. S9 and S10). All of the above significant associations of participation and strength remained significant by partial correlation analysis which controlled for topological covariates (*SI Appendix*, Fig. S11).

We used the Allen Institute data on gene expression in adult wild-type mice to estimate the normalized regional expression of 3,380 genes (all genes which were assayed more than once and passed quality control) (23). We explored the association between gene-expression profiles and nodal participation by using partial least squares, a versatile technique that combines dimensionality

reduction with regression and is well suited for high-dimensional gene-expression data (28). We found that 48% of the variance ($r = 0.69, P < 0.001$) in participation was predicted by a linearly weighted combination of gene expression profiles, such that hi-par hubs overexpressed positively weighted genes (and underexpressed negatively weighted genes) (Fig. 4B). Gene ontology analysis of the top 25% most positively weighted genes demonstrated significant enrichment in three biological processes: cognition, learning and memory, and single organism behavior ($P < 0.001$), and many of the most positively weighted genes are known to be linked to neuronal phenotypes (Fig. 4C and *SI Appendix*, Tables S3 and S5). In contrast, the bottom 25% most negatively weighted genes were not significantly enriched for specific biological processes, although many of these genes have been individually associated with neurodevelopmental phenotypes (*SI Appendix*, Table S4).

Discussion

We have reported an extensive topological and spatial analysis of the tract tracing-based mouse brain connectome. The results showed, in support of our original hypotheses, that the connectome had a complex topology that could not be explained entirely by global minimization of wiring cost. More specifically, high-participation hubs of the connectome mediated many connections between

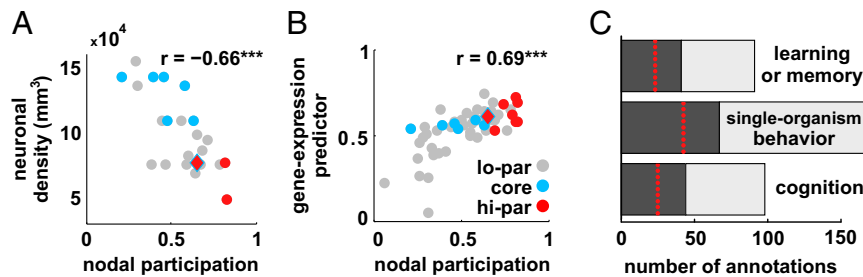


Fig. 4. Histological and gene-expression profiles of hi-par hubs. Scatterplots of participation versus neuronal volume density (A) and partial least squares gene-expression predictor (B). *** $P < 0.001$. (C) The total number of genes annotated for cognition, learning or memory, and single-organism behavior (total length of bars), and the number of annotated genes predictive of participation (dark portion of bars), and the expected number of such genes under the null hypothesis (red dashed lines).

modules, had high axonal wiring costs, slow decay of weight with distance, low neuronal density, high expression of genes enriched for cognitive and behavioral functions, and were not present in cost-minimized network models.

Many aspects of the complex topology revealed by this analysis concur with earlier studies of brain networks. Small-world, hierarchically modular, and core-periphery (alternatively known as rich club) organizations have all been previously reported in graph theoretical analyses of macroscale MRI-based brain networks of humans, and the microscale neuronal network of *C. elegans* (29–31). The hierarchical modular organization is also consistent with prior knowledge of functional localization in the mouse brain. The topological and spatial segregation of visual, auditory, somatosensory, and olfactory regions is not surprising. The auditory-visual module reflects the shared role of auditory and visual cortical areas in monitoring the external environment. Olfactory links to the hippocampus and hypothalamus represent forebrain systems vital to survival for many species in early vertebrate evolution. The integration between mammalian motor and somatosensory cortical systems is strong, and both are linked to the brainstem and cerebellar motor command-and-control systems (25). Moreover, these algorithmically discovered modules accurately reproduce known patterns of developmental gene expression. For example, during early cortical development, the *Fgf8* gene is selectively expressed in rostral (motor, somatosensory, visceral sensory) areas, whereas *Wnt* and *BMP* genes are selectively expressed in caudal (visual and auditory) areas (32). These and other patterns of developmental gene expression are reflected in the segregated modular affiliation of rostral and caudal areas in the adult connectome.

In contrast to the “classical” modules, the hi-par hubs represent a less immediately familiar grouping. Most hi-par hubs correspond to the cortical (anterior cingulate, posterior parietal association, and orbital regions) and subcortical (striatal, diencephalic, and brainstem regions) components of the medial orbital network of the mouse (33). Hi-par hubs also seem to be closely related to the default-mode network (DMN) observed in functional neuroimaging studies of other species (18, 34). For instance, a recent study of the rat brain (34) identified six cortical regions of the DMN (orbital, anterior cingulate, temporal association, posterior parietal association, retrosplenial, and retrohippocampal). In our analysis, three of these regions (posterior parietal association, orbital, and anterior cingulate cortex) were hi-par hubs, two (posterior parietal and auditory association cortex) were in the core, and one (retrohippocampal region) had a high-participation coefficient, but was reliably assigned to a hierarchical module. We additionally found hi-par hubs in subcortical regions (caudate, diencephalon, and midbrain), which are known to be strongly connected to cortical DMN regions (35) but which have not been consistently reported in previous, cortico-centric, functional MRI studies.

We investigated the relationship between topological and spatial features of the connectome by defining the wiring cost of an axonal projection as the product of axonal distance and axonal bandwidth, a marker of axonal cross-sectional area. This cost metric approximates the normalized volume of a cylindrical axonal projection; by this definition, expensive tracts are longer and/or have greater bandwidth. This is an innovative cost metric in mammalian connectomics, because most previous studies have defined wiring cost more crudely as the interregional Euclidean distance, which is bound to underestimate true connection distance (because axonal tracts are often curved rather than straight, *SI Appendix*), and neglects the cost implications of variable bandwidth.

We used this more anatomically accurate measure of wiring cost to show that modules were well approximated by network models that minimized cost, but hi-par hubs could only be generated by a topologically adaptive model that allowed longer distance connections to nodes with high participation. These

observations are compatible with previous models of the connectome based on the trade-off between wiring cost and topological integration (36, 37). Our findings suggest that functionally specialized and anatomically localized modules may be selected by minimization of wiring cost, but hi-par hubs require a competitive selection pressure for topological integration. We further hypothesize that topological integration, by reducing the number of synaptic junctions that must be traversed to pass a message between regional nodes, will tend to reduce conduction delay. In Ramón y Cajal’s language, the conservation of time competes with the conservation of material in the selection of brain networks (1).

It is increasingly important and tractable to understand the neurobiological—genetic, molecular and cellular—correlates of such topological integration (38, 39). We made substantial progress in this direction by reporting associations among nodal participation, low neuronal density, and high expression of genes enriched for cognition, learning and memory, and behavior, and associated with specific neuronal phenotypes. The association between participation and low neuronal density in neocortical regions of the mouse brain is broadly convergent with prior reports of associations between topological centrality and low neuronal density in the macaque connectome (40) and between topological centrality and low cytoarchitectonic differentiation (partly indicative of reduced width, density, and granularity of cortical layer IV) in the cat connectome (41). Reduced neuronal density has been linked to more extensively space-occupying dendritic arborizations and higher synaptic spine counts (42–46). Thus, the observed association between hi-par topology and reduced neuronal density may be mechanistically explicable in terms of greater synaptic density of neurons in hi-par hubs. The association between nodal participation and expression of genes for “higher order” functions provides independent and convergent support for the economical hypothesis that the high cost of topological integration is justified by the role of hi-par hubs in supporting valuable cognitive, learning, and behavioral functions (47).

The Allen Institute has provided one of the largest and richest databases available for any mammalian connectome, but, like any other experimental data, these largely automated measurements are noisy. We applied strict quality control criteria to the tract tracing data to select the most homogeneous injections and applied a probabilistic threshold to eliminate weak and spurious weights. These and other steps in data analysis inevitably involved making assumptions and choices. In particular, there is a trade-off between spatial resolution and signal-to-noise ratio. Finer grained parcellations of the mouse brain are possible and interesting but are also more noisy. To complement the main results, obtained from a relatively coarse-grained but denoised parcellation, we have extensively explored a range of reasonable methodological options in analyzing these data, and whenever possible cross-validated our results with independent datasets. We are confident that our key findings are robustly representative of the organizational principles of the mouse connectome.

We have reaffirmed that complex topology is a general characteristic of brain networks and that wiring-cost minimization is an important but insufficient explanation of mouse brain connectome topology. Our results are compatible with the economical hypothesis—dating back to Ramón y Cajal’s laws of conservation—that nervous systems are selected by competitive pressures for both cost minimization (conservation of material) and topological integration (conservation of time) (48). The adaptive value of expensive but integrative hubs is reinforced by the observation that topological participation is associated with overexpression of genes enriched for higher order cognitive, learning, and behavioral functions.

Materials and Methods

See *SI Appendix*, *SI Materials and Methods* for a full description of materials and methods. The analyses utilized Mouse Connectivity (connectivity.brain-map.org), Developing Mouse Brain (developingmouse.brain-map.org), and

Mouse Brain (mouse.brain-map.org) atlases made freely available by the Allen Institute for Brain Science.

Estimation of Connection Weight. The normalized connection density (NCD) is defined as the number of connections from one unit volume of the source region to one unit volume of the target region (Fig. 1).

Estimation of Wiring Cost. The interregional distance along the axon was estimated by using deterministic tractography on viral tracer projections. The normalized axonal bandwidth from region i to region j , is defined as the fraction of the white-matter boundary of region j , which expressed tracer signal for all experiments in which region i was injected (Fig. 1).

Network Analysis and Modeling. Community and core/periphery structure was detected with a multiresolution consensus-clustering optimization of the modularity and core statistics (49–54). The participation coefficient

quantifies the diversity of nodal intermodular connections (55). Power law and exponential functions for relationships between connection weight (NCD) and axonal distance (millimeters) were fitted by using iteratively reweighted nonlinear least squares.

Correlations. All r values represent Spearman correlation coefficients with P values obtained by using permutation tests.

ACKNOWLEDGMENTS. We thank Petra E. Vértes and Timothy Rittman for suggesting the methods used in the section on gene expression analysis; Terri Gilbert, Manfred Kitzbichler, and Kevin Briggman for helpful discussions; and Olaf Sporns and two anonymous reviewers for constructive comments on drafts. Funding was provided by a NARSAD Young Investigator award and Isaac Newton Trust (to M.R.); a Rubicon Fellowship (to R.J.F.Y.); the Medical Research Council and the Wellcome Trust (Behavioural & Clinical Neuroscience Institute); and the National Institute for Health Research Cambridge Biomedical Research Centre (high-performance computing facilities).

1. Ramón y Cajal S (1995) *Histology of the Nervous System of Man and Vertebrates*, Swanson N, Swanson LW (trans.) (Oxford Univ Press, New York).
2. Catani M, Thiebaut de Schotten M (2012) *Atlas of Human Brain Connections* (Oxford Univ Press, New York).
3. Sporns O, Tononi G, Kötter R (2005) The human connectome: A structural description of the human brain. *PLOS Comput Biol* 1(4):e42.
4. White JG, Southgate E, Thomson JN, Brenner S (1986) The structure of the nervous system of the nematode *Caenorhabditis elegans*. *Philos Trans R Soc Lond B Biol Sci* 314(1165):1–340.
5. Felleman DJ, Van Essen DC (1991) Distributed hierarchical processing in the primate cerebral cortex. *Cereb Cortex* 1(1):1–47.
6. Scannell JV, Young MP (1993) The connectional organization of neural systems in the cat cerebral cortex. *Curr Biol* 3(4):191–200.
7. Stephan KE, et al. (2001) Advanced database methodology for the Collation of Connectivity data on the Macaque brain (CoCoMac). *Philos Trans R Soc Lond B Biol Sci* 356(1412):1159–1186.
8. Van Essen DC, et al.; WU-Minn HCP Consortium (2013) The WU-Minn Human Connectome Project: An overview. *Neuroimage* 80:62–79.
9. Alexander-Bloch A, Giedd JN, Bullmore E (2013) Imaging structural co-variance between human brain regions. *Nat Rev Neurosci* 14(5):322–336.
10. Bullmore E, Sporns O (2009) Complex brain networks: Graph theoretical analysis of structural and functional systems. *Nat Rev Neurosci* 10(3):186–198.
11. Laughlin SB, Sejnowski TJ (2003) Communication in neuronal networks. *Science* 301(5641):1870–1874.
12. Kaiser M, Hilgetag CC (2006) Nonoptimal component placement, but short processing paths, due to long-distance projections in neural systems. *PLOS Comput Biol* 2(7):e95.
13. Budd JM, Kisvárday ZF (2012) Communication and wiring in the cortical connectome. *Front Neuroanat* 6:42.
14. Thomas C, et al. (2014) Anatomical accuracy of brain connections derived from diffusion MRI tractography is inherently limited. *Proc Natl Acad Sci USA* 111(46):16574–16579.
15. Bakker R, Wachtler T, Diesmann M (2012) CoCoMac 2.0 and the future of tract-tracing databases. *Front Neuroinform* 6:30.
16. Kennedy H, Knoblauch K, Toroczkai Z (2013) Why data coherence and quality is critical for understanding interareal cortical networks. *Neuroimage* 80:37–45.
17. Oh SW, et al. (2014) A mesoscale connectome of the mouse brain. *Nature* 508(7495):207–214.
18. Zingg B, et al. (2014) Neural networks of the mouse neocortex. *Cell* 156(5):1096–1111.
19. Markov NT, et al. (2013) The role of long-range connections on the specificity of the macaque interareal cortical network. *Proc Natl Acad Sci USA* 110(13):5187–5192.
20. Markov NT, et al. (2014) A weighted and directed interareal connectivity matrix for macaque cerebral cortex. *Cereb Cortex* 24(1):17–36.
21. Ercey-Ravasz M, et al. (2013) A predictive network model of cerebral cortical connectivity based on a distance rule. *Neuron* 80(1):184–197.
22. Markov NT, et al. (2013) Cortical high-density counterstream architectures. *Science* 342(6158):1238406.
23. Lein ES, et al. (2007) Genome-wide atlas of gene expression in the adult mouse brain. *Nature* 445(7124):168–176.
24. Thompson CL, et al. (2014) A high-resolution spatiotemporal atlas of gene expression of the developing mouse brain. *Neuron* 83(2):309–323.
25. Watson C, Paxinos G, Puelles L (2011) *The Mouse Nervous System* (Elsevier Science, London).
26. Pérez-Escudero A, de Polavieja GG (2007) Optimally wired subnetwork determines neuroanatomy of *Caenorhabditis elegans*. *Proc Natl Acad Sci USA* 104(43):17180–17185.
27. Herculano-Houzel S, Watson C, Paxinos G (2013) Distribution of neurons in functional areas of the mouse cerebral cortex reveals quantitatively different cortical zones. *Front Neuroanat* 7:35.
28. Boulesteix A-L, Strimmer K (2007) Partial least squares: A versatile tool for the analysis of high-dimensional genomic data. *Brief Bioinform* 8(1):32–44.
29. Meunier D, Lambiotte R, Bullmore ET (2010) Modular and hierarchically modular organization of brain networks. *Front Neurosci* 4:200.
30. Towlson EK, Vértes PE, Ahnert SE, Schafer WR, Bullmore ET (2013) The rich club of the *C. elegans* neuronal connectome. *J Neurosci* 33(15):6380–6387.
31. van den Heuvel MP, Kahn RS, Goñi J, Sporns O (2012) High-cost, high-capacity backbone for global brain communication. *Proc Natl Acad Sci USA* 109(28):11372–11377.
32. Fukuchi-Shimogori T, Grove EA (2001) Neocortex patterning by the secreted signaling molecule FGF8. *Science* 294(5544):1071–1074.
33. Ongür D, Price JL (2000) The organization of networks within the orbital and medial prefrontal cortex of rats, monkeys and humans. *Cereb Cortex* 10(3):206–219.
34. Lu H, et al. (2012) Rat brains also have a default mode network. *Proc Natl Acad Sci USA* 109(10):3979–3984.
35. Raichle ME, et al. (2001) A default mode of brain function. *Proc Natl Acad Sci USA* 98(2):676–682.
36. Vértes PE, et al. (2012) Simple models of human brain functional networks. *Proc Natl Acad Sci USA* 109(15):5868–5873.
37. Nicosia V, Vértes PE, Schafer WR, Latora V, Bullmore ET (2013) Phase transition in the economically modeled growth of a cellular nervous system. *Proc Natl Acad Sci USA* 110(19):7880–7885.
38. Wolf L, Goldberg C, Manor N, Sharan R, Ruppin E (2011) Gene expression in the rodent brain is associated with its regional connectivity. *PLOS Comput Biol* 7(5):e1002040.
39. French L, Pavlidis P (2011) Relationships between gene expression and brain wiring in the adult rodent brain. *PLOS Comput Biol* 7(1):e1001049.
40. Scholtens LH, Schmidt R, de Reus MA, van den Heuvel MP (2014) Linking macroscale graph analytical organization to microscale neuroarchitectonics in the macaque connectome. *J Neurosci* 34(36):12192–12205.
41. Beul SF, Grant S, Hilgetag CC (2014) A predictive model of the cat cortical connectome based on cytoarchitecture and distance. *Brain Struct Funct*, 10.1007/s00429-014-0849-y.
42. Schüz A, Palm G (1989) Density of neurons and synapses in the cerebral cortex of the mouse. *J Comp Neurol* 286(4):442–455.
43. Collins CE, Airey DC, Young NA, Leitch DB, Kaas JH (2010) Neuron densities vary across and within cortical areas in primates. *Proc Natl Acad Sci USA* 107(36):15927–15932.
44. Jacobs B, et al. (2001) Regional dendritic and spine variation in human cerebral cortex: A quantitative golgi study. *Cereb Cortex* 11(6):558–571.
45. Cullen DK, Gilroy ME, Irons HR, Laplaca MC (2010) Synapse-to-neuron ratio is inversely related to neuronal density in mature neuronal cultures. *Brain Res* 1359(0):44–55.
46. Ivenshtiz M, Segal M (2010) Neuronal density determines network connectivity and spontaneous activity in cultured hippocampus. *J Neurophysiol* 104(2):1052–1060.
47. Warren DE, et al. (2014) Network measures predict neuropsychological outcome after brain injury. *Proc Natl Acad Sci USA* 111(39):14247–14252.
48. Bullmore E, Sporns O (2012) The economy of brain network organization. *Nat Rev Neurosci* 13(5):336–349.
49. Newman MEJ, Girvan M (2004) Finding and evaluating community structure in networks. *Phys Rev E Stat Nonlin Soft Matter Phys* 69(2 Pt 2):026113.
50. Reichardt J, Bornholdt S (2006) Statistical mechanics of community detection. *Phys Rev E Stat Nonlin Soft Matter Phys* 74(1 Pt 2):016110.
51. Blondel VD, Guillaumet JL, Lambiotte R, Lefebvre E (2008) Fast unfolding of communities in large networks. *J Stat Mech* 2008:P10008.
52. Sun Y, Danila B, Josić K, Bassler KE (2009) Improved community structure detection using a modified fine-tuning strategy. *Europhys Lett* 86(2):28004.
53. Lancichinetti A, Fortunato S (2012) Consensus clustering in complex networks. *Sci Rep* 2:336.
54. Borgatti SP, Everett MG (2000) Models of core/periphery structures. *Soc Networks* 21(4):375–395.
55. Guimerà R, Amaral LAN (2005) Cartography of complex networks: Modules and universal roles. *J Stat Mech* 2005(P02001):a35573.